Proceedings of the 6th International Conference on Gas Hydrates (ICGH 2008),
Vancouver, British Columbia, CANADA, July 6-10, 2008.

FLUID FLOW THROUGH HETEROGENEOUS METHANE HYDRATE-BEARING SAND: OBSERVATIONS USING X-RAY CT SCANNING

Yongkoo Seol*
National Energy Technology Laboratory
US Department of Energy
3610 Collins Ferry Road, Morgantown, WV 26507
USA

Timothy J. Kneafsey
Earth Science Division
Lawrence Berkeley National Laboratory
One Cyclotron Road, Berkeley, CA 94720
USA

ABSTRACT

The effects of porous medium heterogeneity on methane hydrate formation, water flow through the heterogeneous hydrate-bearing sand, and hydrate dissociation were observed in an experiment using a heterogeneous sand column with prescribed heterogeneities. X-ray computed tomography (CT) was used to monitor saturation changes in water, gas, and hydrate during hydrate formation, water flow, and hydrate dissociation. The sand column was packed in several segments having vertical and horizontal layers with two distinct grain-size sands. The CT images showed that as hydrate formed, the water and hydrate saturations were dynamically redistributed by variations in capillary strength of the medium (the tendency for a material to imbibe water), which changed with the presence and saturation of hydrate. Water preferentially flowed through fine sand near higher hydrate-saturation regions where the capillary strength was elevated relative to the lower hydrate saturation regions. Hydrate dissociation initiated by depressurization varied with different grain sizes and hydrate saturations.

Keywords: methane hydrate, sediment heterogeneity, x-ray computed tomography

INTRODUCTION

Gas hydrate formation, dissociation, and fluid flow through a porous medium with hydrate are of interest to a wide range of applications. Natural gas hydrates (referred to herein as "hydrates") have recently attracted attention as a possible energy resource [1, 2] and a potential contributor to global warming via methane gas release [3-6]. To assess the potential of hydrates as an energy resource or environmental hazard, the behavior of hydrates in sediments needs to be clearly understood. The effects of hydrate saturation and distribution on the capillary pressure, relative permeability, and geomechanical properties of sediment are not well documented. In addition, the presence of heterogeneity in the sediment where hydrate forms adds complexity to understanding the behavior of hydrate-bearing sediment.

Experiments performed to characterize the properties of hydrate-bearing sand have focused primarily on thermodynamic properties [7-16]. However, most of those studies were limited to homogeneous media, in order to simplify the

* Corresponding author: Phone: +1 304 285 2029 Fax +1 304 285 0903 E-mail: yongkoo.seol@netl.doe.gov

system, even though uniform media are not always representative of natural conditions. We formed methane hydrate in a heterogeneous sand column with prescribed heterogeneities to observe the effects of heterogeneity on hydrate formation, water flow through the heterogeneous hydrate-bearing sand, and hydrate dissociation. Our sand pack contained two grain-size ranges of a silica sand, providing a permeability and capillary pressure contrast between layers, and was packed in layers varying in direction with respect to gravity and the column axis (i.e., perpendicular or parallel). X-ray computed tomography (CT) scanning was used to gather high-resolution density data, which was then converted to porosity and phase saturations (water and hydrate). In addition, temperature, and pressure were measured to monitor conditions in the sample. The observations and measurements related to this heterogeneous system, even though drastically simplified, will aid in refinement of conceptual models of gas and water flow in hydrate-bearing porous media, and in predicting how natural heterogeneity in hydrate-bearing reservoirs can affect fluid movement and natural gas production.

EXPERIMENTAL METHOD

The experiment consisted of five phases: (1) sand column packing and flow-system setup; (2) methane hydrate formation; (3) water flooding; (4) hydrate dissociation by depressurization; and (5) column saturation with water and subsequent drying to provide density reference data for phase saturation calculations. The CT scans were conducted during each experimental phase to (1) image saturation changes upon hydrate formation and dissociation, (2) infer water and gas migration in response to hydrate formation and dissociation, and (3) observe water flow through the medium with heterogeneous hydrate saturation.

Sand Column and Flow System Preparation

The pressure vessel used in this experiment was a 76.2 mm inside diameter, 89 mm outer diameter, aluminum tube with threaded stainless steel end caps (Figure 1). Prior to packing the sand in the pressure vessel, the outlet end cap, equipped with three Type-K thermocouples (Omega Engineering, Stamford, CT), a 6.4 mm thick neoprene foam pad, and a 12.8 mm thick solid Teflon spacer (to provide a cushion and thermal insulation between the sample and the stainless steel end cap) was attached to the aluminum tube.

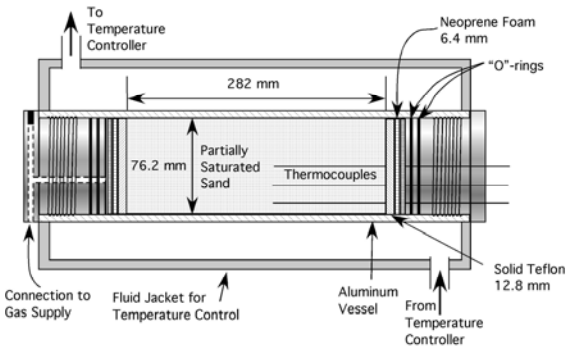

Figure 1. Experiment system schematic

Silica sand (U.S. Silica F110, Berkeley Springs, WV) was sieved into two size fractions: fine grain sand (53–177 μm) and coarse grain sand (177–295 μm). The sand was selected because of its rounded, regular grain shape. These two sand fractions were washed with deionized water and air-dried before use. Following drying, they were moistened with distilled deionized water, resulting in the mass ratio of water to sand of 0.066 for both sands.

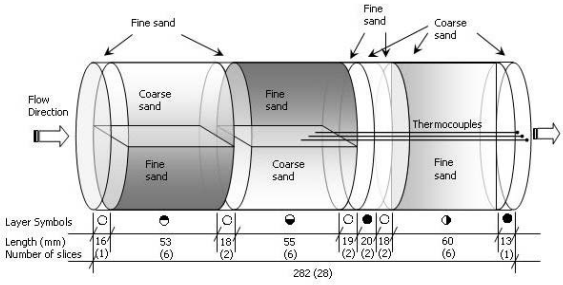

Figure 2. Layer configuration in the sand pack. Each layer is identified by layer symbols consisting of an open area (fine-grain sand) and a filled area (coarse-grain sand). Numbers at the bottom are the lengths of each segment in millimeters with the number of CT slices in parentheses.

The two sands were packed into the pressure vessel according to the layer configuration shown in Figure 2. The vessel was oriented vertically during packing, and the sand was packed into the vessel from the outlet to the inlet end in approximately 1 cm thick lifts, and tamped into place using various diameter rods to ensure uniform packing. Upon filling the vessel to the appropriate level, a matching Teflon spacer and neoprene foam pad were inserted on the top of the

sand pack followed by the stainless steel end cap. The resulting sand column was 282 mm in length and 76.2 mm in diameter. Finally, the packed pressure vessel was oriented horizontally and allowed to equilibrate for three days prior to hydrate formation.

The sand column had four main segments (Figure 2). Proceeding from the inlet end, and given the final horizontal orientation of the column, they are (1) horizontal layers with coarse sand on top, (2) horizontal layers with fine-grain sand on top, (3) alternating fine/coarse/fine vertical layers perpendicular to the vessel axis, and (4) vertically divided layers with fine sand on the thermocouple side of the column. The first two segments were separated by a thin (~1 cm) fine sand layer, as shown in Figure 2. A thin fine sand layer at the inlet end and between the major segments was used to provide uniform flow to the adjacent column segment, and a thin coarse sand layer was placed at the outlet end to reduce the capillary barrier for water at the exit. The three thermocouples were situated on the boundary between the fine and coarse sands in the second horizontally oriented segment.

The pressure vessel was fitted into a PVC jacket through which temperature-controlled fluid (water/ethylene glycol) was circulated to control the system temperature. The inlet end of the pressure vessel was connected to a 3.8 L steel bottle and an Isco 500D syringe pump (Lincoln, NE) used to control flow during the experiment. Both the bottle and the Isco pump were connected to various gas cylinders (CH_4, N_2, or CO_2) when needed. The outlet end of the pressure vessel was also connected to an Isco 500D syringe pump and a back-pressure regulator. Pressures were monitored at the two pumps, the vessel inlet, and the differential pressure across the sample while temperatures were measured in the room, the temperature-controlled bath, the sample at three locations, and the steel bottle containing methane gas.

The pressure vessel with the water jacket was insulated to minimize external thermal influences and mounted at a fixed location on the x-ray CT scanner table to reduce table-positioning errors. A modified Siemens HiQ medical x-ray CT scanner was used to obtain CT images. Sequential 10 mm thick cross sectional images were collected over the length of the sample (28 slices). The voxel size for the CT images for this test was ~0.24 × 0.24 × 10 mm; 371 × 371 voxels per slice are presented in the images shown. The CT scans were performed periodically, including before and after hydrate formation, during the water flood, during dissociation, while the sample was water-saturated, and while it was completely dry.

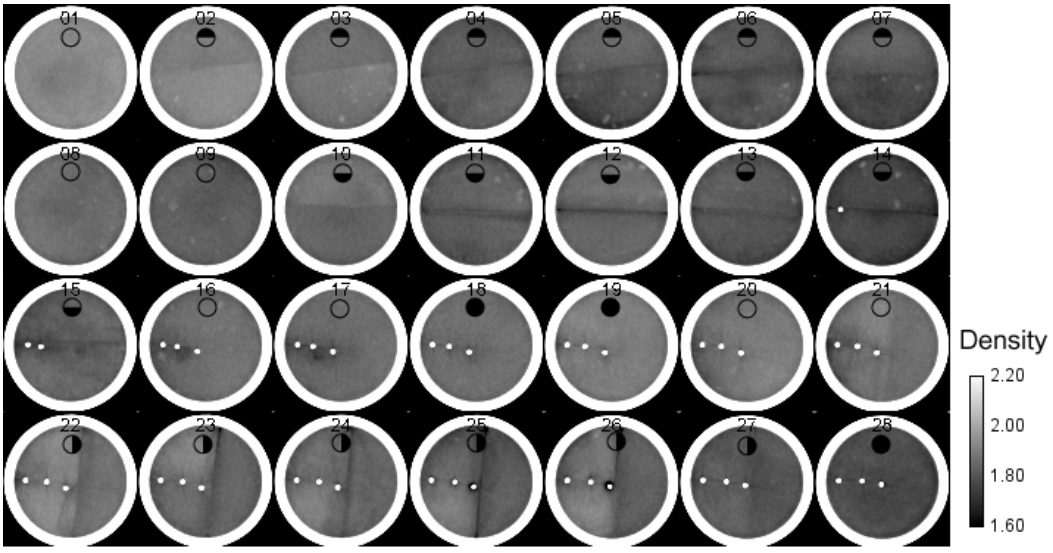

Figure 3. CT images showing initial conditions prior to hydrate formation. The number on the top is the slice number starting from the inlet end. Circles just below the slice number on each image represent the layer configuration, with the open area representing fine sand and the filled area representing coarse sand.

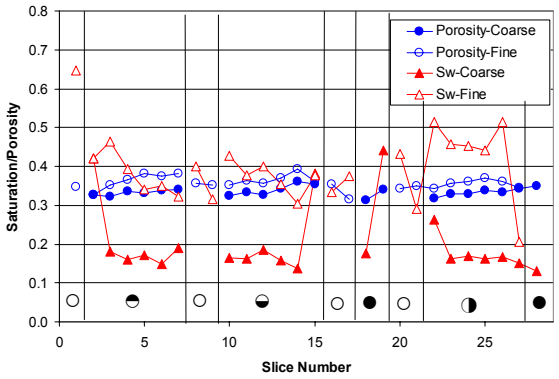

Figure 4. Average water saturation and porosity for each layer. The two sands (with different grain sizes) were separately averaged. Vertical lines show the location of column segment (or layer) boundaries.

Figure 3 presents the 28 CT images comprising the sample, showing the initial condition and the horizontal or vertical layer boundaries as specified in Figure 2. Each voxel of the CT images represents the average density for a 1 cm slice of the sand calibrated from materials with known density. The varying density shown in the images resulted from slightly non-uniform packing and variations in water saturation due to corresponding variations in capillary strength. Here we refer to capillary strength as a measure of the tendency for a material to imbibe water. Capillary strength increases in water-wetting media with smaller pore sizes, such as in regions with a tighter grain packing and in sand with smaller grain sizes. This results in higher water saturation in these regions. Small white circles appearing in the interior of Slices 14 through 28 identify the three thermocouples. As calculated from the CT images, the average initial porosity ranges between 0.33 and 0.40, and the average water saturation ranges between 0.15 and 0.5 (Figure 4).

Hydrate Formation

Hydrate was formed by pressurizing the sample at a fixed temperature to an appropriate pressure within the hydrate stability region. We initially set the temperature to 4°C and the methane gas pressure was raised to 4.8 MPa (700 psi) to form the hydrate, but because hydrate did not begin to form in two days, we lowered the temperature to 3ºC and raised the methane gas pressure to 5.5 MPa (802 psi) to expedite the hydrate-forming process. Hydrate began to form about 12 hours after the change in conditions. The completion of hydrate formation was identified by stable pressure and temperature inside the pressure vessel.

Water Flood

Deionized water was injected into the sand column at a rate of 4.0 mL/min using the syringe pump. Injected water temperature was not separately controlled, because it was expected that the water would be thermally equilibrated while flowing through the massive pressure vessel end piece, which was within the temperature controlled region. X-ray CT scans were taken at three specific locations (Slices 7, 13, and 23) during the waterflood rather than throughout the entire column with the observed slices representing each of the main column segments. The changes in water saturation as the water flood progressed were calculated based on the assumption that the hydrate present in the sand column was stable, neither forming nor dissociating. The temperature-pressure conditions were constant and within the hydrate stability region [3ºC and 700 psi (4.83 MPa)].

Hydrate Dissociation

We used a back-pressure regulator to control pressure during hydrate dissociation. The outflow from the vessel (mostly gas with a small quantity of water) was flowed into a Marriott collection bottle for gas quantification. Hydrate dissociation was initiated by slowly lowering the sample pressure, but not so low as to cause the formation of ice. The pressure inside the vessel was 691 psi (4.76 MPa) before depressurization, and the back-pressure regulator kept the pressure at 520 psi (3.59 MPa) until the hydrate was dissociated, after which the pressure was slowly lowered to atmospheric pressure. During dissociation, CT scans of every other 1 cm thick slice over the entire sample (14 slices) were performed every 10 to 13 minutes to monitor the changes in density.

Saturated and Dry Sand Column

CT images of the sand column under water-saturated and completely dry conditions provide the best endpoints for computing hydrate and fluid saturations during other stages of the experiment. For this purpose, the sand column was fully saturated with water, scanned, completely dried, and scanned again after hydrate formation and dissociation. During the water saturation, some gas was unintentionally injected into the column,

causing a disturbance in the sand packing in the first few slices. This, in turn, impacted the calibrations in those affected slices, as shown in Figures 5 and 8.

RESULTS and DISCUSSION

Sand Column

Table 1 shows the average porosities and fluid saturations calculated from the CT images. The porosity of the coarse sand is lower than that of the fine sand, and consequently the bulk density of the coarse sand is higher than the fine sand. However, the initial water saturation (0.40) in the fine sand is much higher compared to the coarse sand (0.18) (Figure 4), because of the higher capillary strength.

Hydrate Formation

Figure 5 shows hydrate saturation following formation. Hydrate saturation was calculated based on the x-ray attenuation values, which were compared to fully water-saturated and completely dry sand CT images collected after completion of hydrate dissociation. Figure 6 shows the average saturations of hydrate and water for both sands for each slice.

The hydrate saturation in the fine sand exceeded that in the coarse sand (Table 1 and Figures 5 and 6). This finding was expected, because hydrate saturation is closely related to the initial water saturation, and because the initial water saturation in the fine sand is significantly greater than that of the coarse sand. However, in the fine sand, the hydrate saturation (0.35) was less than the expected hydrate saturation (0.39) calculated from the consumed water saturation (0.40–0.09=0.31) and volume expansion factor (1.265). In the coarse sand, the hydrate saturation (0.28) was higher than the expected hydrate saturation (0.13) (Table 1). These observations confirm that as hydrate forms, water redistributes according to changing capillary strengths [8, 17-18], and that hydrate formation caused imbibition of water into regions where the sand was initially drier.

Average	Coarse Sand	Fine Sand
Grain Size, μ	177-259	53-177
Bulk Density, ρ	1.776	1.719
Porosity, ϕ	0.34	0.37
Initial Water Saturation (after equilibration), S_{wo}	0.18	0.40
Hydrate Saturation, S_h	0.28	0.35
Water Saturation (in the presence of hydrate), S_W	0.075	0.093

Table 1 Average properties and saturations in the sands calculated using CT data

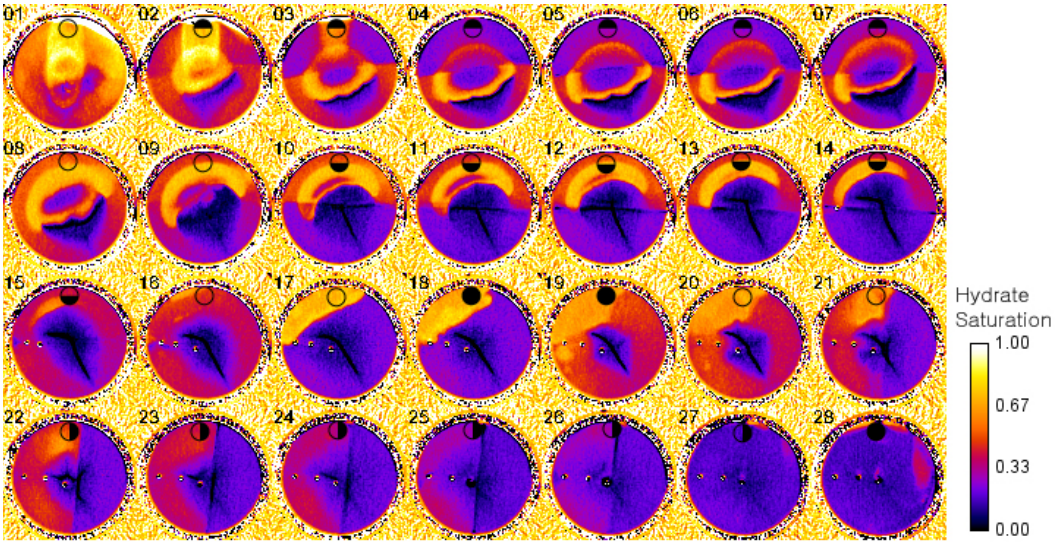

Figure 5. CT images showing hydrate saturation after the completion of hydrate formation.

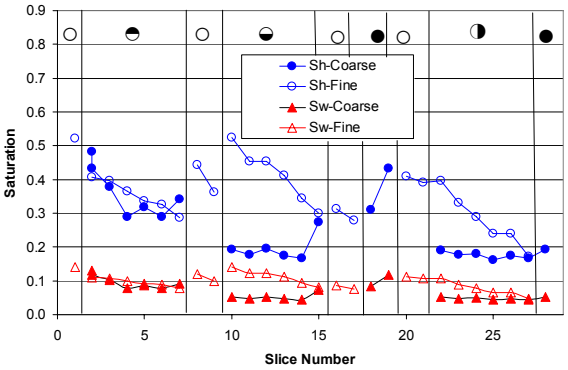

Figure 6. Average water saturation and measured hydrate saturation on each slice.

Hydrate saturation is more uniform in the coarse sand, but more highly localized in the fine sand. The fine sand contains a much less saturated region below the highly concentrated hydrate region (Figure 5). The average hydrate saturation is highest (~53% at Slice 10) in the fine sand in the middle segment, and decreases to below 30% at Slice 15 (in the same segment). Average hydrate saturation in the coarse sand ranges from about 30 to 50% in the first segment and 17 to 20% in the rest of the column, except for Slices 15, 18, and 19, located at the boundary with fine sand. The highest hydrate saturation in the coarse sand (44%) was found in the vertical layer (Slices 18 and 19) located between the two vertical fine layers in the middle of the column. This layer had the highest initial water saturation for the coarse sand as well.

Images of hydrate saturation in Figure 5 suggest that there are two contrasting regions in the column in terms of hydrate saturation, one from Slices 1 to 15 and the other from Slices 16 to 28. In the first half, hydrate forms in circular band shaped as half rings, while in the second half, the hydrate is more or less locally concentrated (e.g., Slices 17 and 18) or uniformly disseminated. The complex behavior observed during hydrate formation is still incompletely understood. While the circular band-like hydrate formation has been observed in other experiments [18], it is not completely understood.

Slices 10 to 15 (Figure 5) show a concentrated hydrate zone and water-depleted zone in the fine sand. However, the coarse sand did not show a high hydrate-saturation band. Instead, a crack-like low-density area extending through Slice 21 formed. According to the densities estimated from the CT images, this narrow crack-like region is not void space, but a low-density area. The density in the crack region was about 1.62 g/cm^3, while the density of the dry sand in the same area was about 1.72 g/cm^3. In this region, water may have been depleted, lowering capillary adhesion between grains, so that water could not hold the sand particles together. The water presumably migrated from the region to the location where hydrate was forming. At Slice 18, the expected hydrate saturation in the coarse sand (based on the initial water saturation and residual water saturation) would be about 13% (Figure 4), but the actual hydrate saturation is about 31% (Figure 6). These findings indicate that a significant volume of water migrated into the coarse region.

In the segment between Slices 22 and 27, the boundary separating the different grain-size sands has a lower density than the surrounding sands, which could result in similar fluid-flow behavior as the crack-like region in Slices 10 to 21. The circular banded hydrate-formation pattern was not observed here, because water may have flowed parallel to the column axis in this region. The water in this region may have migrated into the alternating vertical layers (Slices 17 to 21) where the hydrate saturation was higher than expected (Figure 6).

Water Flood

We monitored the water flood using CT to identify the dominant flow pathways through the hydrate-bearing sediments. Information on water flow through such heterogeneous hydrate-bearing sediment enhances our understanding of the flow of water released from hydrate dissociation when a hydrate reservoir is under development for natural gas.

Figure 7 shows the changes in saturation at three locations in the sample during the water flood. The three locations were selected to examine the effects of grain size and hydrate saturation on water flow through the three regions, and the third location was specifically selected to track the gravity effect on water flow through the region having vertically oriented coarse and fine layers in the axial direction. Vertical fine sand layers placed between the three major column segments were designed to act as flow buffer zones, providing relatively uniform water inflow to subsequent

column segments. However, the hydrate saturation in these layers was observed to be heterogeneous as well, with the distributions resembling those of the nearby segments; thus, homogeneous flow redistribution was unlikely.

The top 14 images in Figure 7 show the water saturation changes in the segment (Slice 7) having the coarse sand over the fine sand with a nearly horizontal boundary. The inflow of water appeared immediately beneath the high-hydrate-saturation zone in the fine sand, where capillary strength would be high and permeability would be highest. Water first filled the lower fine sand and then later slowly imbibed upward into the coarse sand-more readily through the higher hydrate-saturation zone, which had increased capillary strength. A low-density region in the center of the column remained nearly unchanged after water was introduced into the column. The central low-density region may have resulted from rearrangement of sand particles as hydrate formed, or from trapped gas from flow-path blockages caused by residual water or hydrate formed at pore throats.

The second set of images in Figure 7 shows the flow pattern in the horizontal layers of the second segment (Slice 13), with the upper fine-grain sand. The water breakthrough first appeared in the fine sand just beneath the high hydrate-saturation region as in the first segment, and later propagated to the lower coarse sand while also flowing upwards around the high hydrate-saturation region. After the complete satiation (not necessarily saturated, but unable to imbibe more water) of the section, there was a slightly less saturated region left in the fine sand in the center of the high hydrate-saturation region, where the circular band-shaped high-hydrate density region pinches out. This region seems isolated by what may be pore-blocking hydrate formation from outside water flow. The low density crack-like region found on the lower coarse sand is one of the last regions of the coarse sand to fill, since it has a lower capillary strength.

The bottom set of images in Figure 7 shows the water breakthrough in the sand layers having a vertical contact boundary with the fine sand on the left (Slice 23). Hydrate saturation in this segment was relatively uniform in both the fine and coarse sand, and the water breakthrough occurred in the center of the fine sand, where the hydrate saturation was lower. The vertical boundary between the two sands seems to impose a capillary barrier, hindering water flow between the two sides. After the fine sand was nearly satiated, the coarse sand started to fill up from the bottom. When the entire coarse sand section was nearly satiated, the top portion of the fine sand was still not fully satiated. The area could be similarly isolated by pore clogging with hydrate saturation.

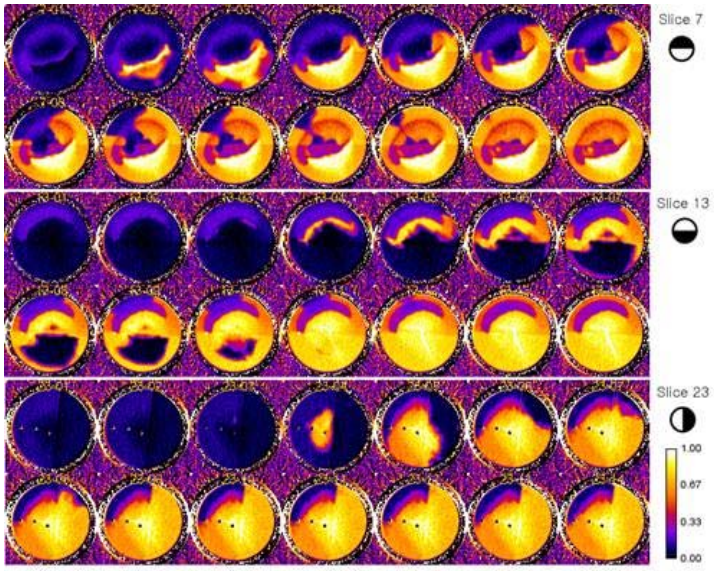

Figure 7. CT images showing water breakthrough at Slices 7, 13, and 23. The 14 images in each set for a slice show the temporal evolution of water saturation.

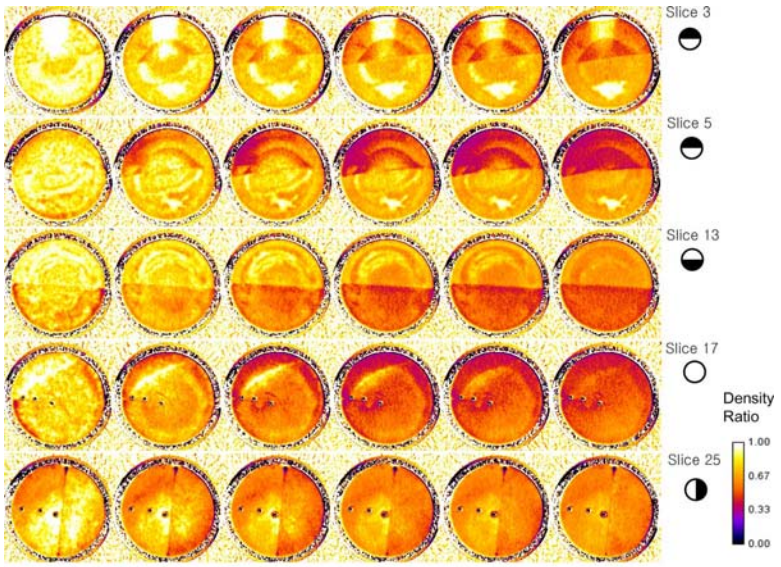

Figure 8. CT images showing effects of hydrate dissociation as the density ratio (DR) of the measured density to the water-saturated density at Slices 3, 5 13, 17, and 25.

Hydrate Dissociation

Depressurization was employed to induce hydrate dissociation in the water-satiated hydrate-bearing sand. During dissociation, there was no flow through the inlet, and fluids were removed through the outlet. Hydrate dissociation requires heat input regardless of the method used. Depressurization causes the initial dissociation to occur throughout the sample from the heat already present in the sample, before heat transfer from outside the sample is required.

We use the density ratio (DR) – the ratio of the measured density at a particular location and time to the density of that same location of the water-saturated sample – to help interpret dissociation. Figure 8 shows the DR for five cross sections over time as the hydrate dissociated. The time between sequential images (left to right) is approximately 20 to 25 min. In this figure, darker regions contain sand with less dense components – gas and hydrate, and the brighter regions contain sand with the more dense component – water. During dissociation, the different sand segments showed dissimilar trends. In the coarse sand (see the top layer of Slices 3 and 5), the hydrate in the high hydrate-saturation region (circular band, see Figure 5) dissociated faster (becoming darker earlier) than the hydrate in the fine sand. The hydrate in the high-hydrate-concentration region in the fine sand persisted longer. Similar behavior was observed in Slice 13, where in the fine sand (top), the region of higher hydrate saturation (see Figure 5) remains longer during hydrate dissociation, and the coarse sand with the low uniform hydrate saturation (Figure 5) dissociates fairly uniformly. These unequal dissociation rates in the different sands may result from varying permeability because the reduction of permeability associated with high hydrate saturations, or may result from the higher hydrate saturations in these locations. Dissociation in Slice 17, having only fine sand, occurs radially from the outside-in, however the crescent-shaped highly hydrate saturated region along the top left persists as long as the highly hydrate saturated regions in the other segments. Hydrate in the vertically oriented slices (Slice 25 in Figure 8) was primarily uniform, and dissociation occurred radially inwards from the vessel wall.

We did not observe preferential pathways for fluid flow from released water and gas. In the fine sand, an irregular area of high density (i.e., high water saturation) appeared in the lower central region (see Slices 3 and 5). This region is in the same area where water was depleted during hydrate formation and then filled with water during the waterflood. Since the region contained little hydrate to begin with, it remained high in water saturation because little gas was produced there.

As the hydrate dissociated, the crack-like low-

density region, which developed upon hydrate formation (dark line in Figure 8, Slice 17 and Figure 5, Slices 10-21) disappeared. This disappearance may have resulted from the disaggregation of sand particles associated with hydrate and rearrangement of sand particles with fluid released from dissociating hydrate, or from water being reintroduced into this region after it had become extremely dry upon hydrate formation.

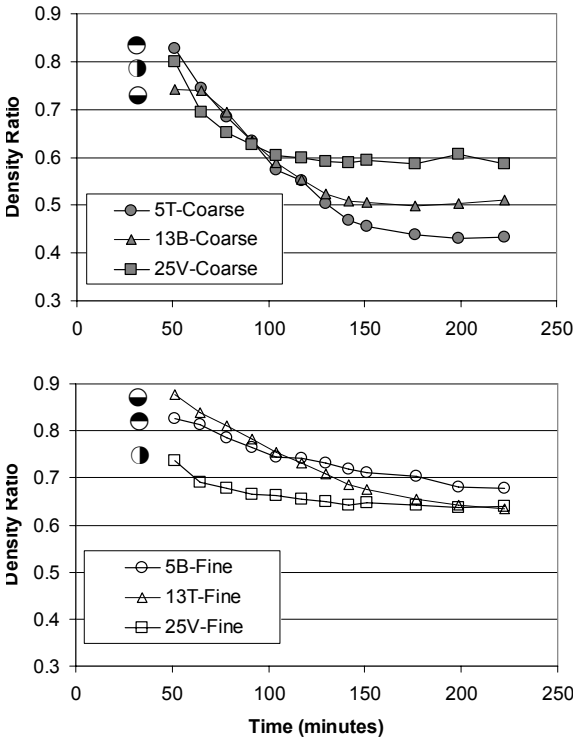

Figure 9. Density ratio during hydrate dissociation monitored at Slices 5, 13, and 25. "T,""B," and "V" stand for top, bottom, and vertical layer.

Figure 9 shows the variations in the DR over time for three locations during dissociation. Over time, the fine-sand DR became relatively uniform throughout the column, even though the initial DRs were varied. The coarse sand shows the opposite trend, with a varying final mass ratio at different locations as time progressed. The varying final DR in the coarse sand suggests that the gas and water released from hydrate dissociation were ushered toward the outlet, and water accumulated in the region closer to the outlet, whereas the inlet end remained more highly saturated with gas. The fine sand with higher capillary strength maintains a higher and more uniform water saturation. The magnitude of the decline in DR is also different for each sand—the final DR in the fine sand is approximately 0.65, whereas in the coarse sand, the final DR ranges from 0.43 to 0.6, indicating a greater accumulation of gas in the coarse sand.

CT images (not shown) of the saturated and dried conditions after hydrate dissociation appear uniform and show no signs of permanent density changes resulting from hydrate formation or remnants of the crack.

SUMMARY

A water flow experiment was performed to observe hydrate formation and dissociation, as well as water flow in a heterogeneous sand column with known heterogeneity. In our experiment, hydrate formed more predominantly in regions where water saturation was high. It formed relatively uniformly in coarse sand, but was more strongly localized in the fine sand, possibly because of the higher effective permeability of the fine sand, resulting from the higher water saturation within it. When hydrate formed, crack-like low-density regions developed, affecting water imbibition and migration.

Water flow through hydrate-bearing sands was also observed. Water was imbibed more readily into the fine sand near high hydrate-saturation regions, suggesting that the formation of hydrate increased the capillary strength. Hydrate dissociation initiated by depressurization varied with different grain sizes, permeabilities, and capillary strengths. Because high hydrate-saturation regions in the fine sand may buffer the impact of an imposed pressure drop, the dissociation rate in those regions was slower compared to their surroundings.

We have observed various features in the CT images, including the circular patterns of hydrate formation and concentrated local high hydrate saturation. Further studies will be conducted to understand the features occurring with hydrate formation and dissociation.

ACKNOWLEDGMENTS

The authors wish to acknowledge Dan Hawkes for their helpful review on this manuscript. This work was supported by the Assistant Secretary for Fossil Energy, Office of Natural Gas and Petroleum Technology, through the National

Energy Technology Laboratory, under the U.S. DOE Contract No. DE- AC02-05CH11231, and also in part by the Korean Institute of Geoscience and Mineral Resources.

REFERENCES

[1] Sloan, E.D., 1998. Clathrate Hydrates of Natural Gases, second ed. Marcel-Dekker, Inc, New York. 705 pp.

[2] Makogon, Y.F., 1987, Gas hydrate: frozen energy, Recherche 18(192), 1192

[3] Klauda, J.B., S.I. Sandler, 2005. Global distribution of methane hydrate in ocean sediment. Energy and Fuels,19, 459

[4] Milkov, A.V., R. Sassen, 2003. Two-dimensional modeling of gas hydrate decomposition in the northwestern Gulf of Mexico: Significance to global change assessment. Global and Planetary Change36, 31

[5] Milkov, A. V. Global estimates of hydrate-bound gas in marine sediments: how much is really out there? Earth Science Reviews 2004, 66, 183

[6] Ruppel, C. Natural gas hydrate in oceanic and permafrost environments, Max Ed. 2000, Book, 29

[7] Gupta A., Timothy J. Kneafsey, George J. Moridis, Y. Seol, Michael B. Kowalsky, and E. D. Sloan, Jr. 2006, Composite Thermal Conductivity in a Large Heterogeneous Porous Methane Hydrate Sample. *Phys. Chem. B,* 110 (33), 16384 - 16392, 2006

[8] Moridis, G.J., Y. Seol and T. Kneafsey, Studies of reaction kinetics of methane hydrate dissociation in porous media, *Fifth International Conference on Gas Hydrates,Trondheim, Norway* 2005, *1004*, 21.

[9] Handa, Y.P., Stupin, D., 1992. Thermodynamic properties and dissociation characteristics of methane and propane hydrates in 70A radius silica gel pores. J. Phys. Chem. 96, 8599

[10] Huang, D., Fan, S., 2005. Measuring and modeling thermal conductivity of gas hydrate-bearing sand. J. Geophys. Res. 110 (B01311)

[11] Klapproth, A., K.S. Techmer, S. A. Klapp, M. M. Murshed, and W. F. Kuhs, 2006. "Microstructure of gas hydrates in porous media", *Proceedings of the 11th International Conference on the Physics and Chemistry of Ice*, Bremerhaven, July 23 - 28, 2006, Royal Society of Chemistry

[12] Lu, H. and R. Matsumoto, 2002. Preliminary experimental results of the stable P_T conditions of methane hydrate in a nannofossil-rich claystone column, Geochemical Journal, v 36, pp. 21-30

[13] Santamarina, J. C., F. M. Francisca, T. S. Sun, J. Y. Lee, A. I. Martin, and C. Ruppel 2004. Mechanical, thermal, and electrical properties of hydrate bearing sediments", *AAPG Hedberg Conference*, Vancouver, BC, Canada, AAPG.

[14] Waite, W.F., Winters, W.J., Mason, D.H., 2004. Methane hydrate formation in partially water-saturated Ottawa sand. Am. Mineral. 89, 1202.1207

[15] Uchida, T, S. Takeya, E. Chuvilin, R. Ohmura, J. Nagao, V. Yakushev, V. Istomin, H. Minagawa, T.Ebinuma, and H. Narita, 2004. Decomposition of methane hydrates in sand, sandstone, clays, and glass beads, Journal of Geophysical Research, v 109, B05206, doi:10.1029/2003JB002771

[16] Uchida, T., T. Ebinuma, S. Takeya, J. Nagao, and H. Narita, 2002. Effects of pore size on dissociation temperatures and pressures of methane, carbon dioxide, and propane hydrates in porous media, Journal of Physical Chemistry B, v 106, pp. 820-826

[17] Kneafsey, T.J., Tomutsa, L., Taylor, C.E., Gupta, A., Moridis, G., Freifeld, B. and Seol, Y., 2005. Methane hydrate formation and dissociation in a partially saturated sand, The 229th ACS National Meeting, San Diego, CA, LBNL-56933 Ext. Abs.

[18] Kneafsey, T.J., L. Tomutsa, G.J. Moridis, Y. Seol, B.M. Freifeld, C.E. Taylor, and A. Gupta, 2007, Methane Hydrate Formation and Dissociation in a Core-Scale Partially Saturated Sand Sample, Journal of Petroleum Science and Engineering, 56, 2007 108-126